

NANO EXPRESS

Open Access



Atomic Layer Deposition of Pt Nanoparticles for Microengine with Promoted Catalytic Motion

Chi Jiang¹, Gaoshan Huang^{2*}, Shi-Jin Ding³, Hongliang Dong², Chuanling Men¹ and Yongfeng Mei^{2*}

Abstract

Nanoparticle-decorated tubular microengines were synthesized by a combination of rolled-up nanotechnology and atomic layer deposition. The presence of Pt nanoparticles with different sizes and distributions on the walls of microengines fabricated from bilayer nanomembranes with different materials results in promoted catalytic reaction efficiency, which leads to an ultrafast speed (the highest speed 3200 $\mu\text{m/s}$). The motion speed of the decorated microengines fits the theoretical model very well, suggesting that the larger surface area is mainly responsible for the acceleration of the motion speed. The high-speed nanoparticle-decorated microengines hold considerable promise for a variety of applications.

Keywords: Microengine, Atomic layer deposition, Pt nanoparticles, Surface area

Background

The syntheses of micro-/nano-engines that are able to perform various tasks have attracted great attention with the development of nanotechnology. Among these artificial engines, catalytic micro-/nano-engines with different shapes of rod [1], sphere [2], helical [3], and tubes [4], mimicking their counterparts in the nature [5], are capable of moving autonomously in the presence of corresponding fuels or powered by various external stimuli such as light [6], magnetic [7], or ultrasound fields [8]. Particularly, bubble-propelled tubular microengines have become highly attractive due to their impressive features including high-power output, ultrafast movement speed, and independence of motion on ionic strength in liquid media [9]. In order to fabricate microtubular structures with catalytic inner surfaces, different methods have been employed, including template electrodeposition methods using porous membranes [10, 11] and roll-up technology [12]. Rolled-up technology have a few advantages like wide range of materials engaged and easy tuning of length and diameter [12], and the fabricated microengines have been applied to cargo-towing [13], tissue-drilling [14], dynamic assembly [15], and so on.

With further development of micro-/nano-electromechanical system, powerful micro-/nano-engines with high speed and large driving force are demanded to accomplish complex tasks by overcoming the viscous force at low Reynolds number [16], and various measures have been applied to improve the performance of the catalytic microengines. For instance, graphene [17], carbon nanotube [18], and nanoparticles [19] have been used to promote catalytic reactions, and the hierarchical nanoporous microtubular engines [20] have been reported to improve fuel refilling. Although these methods can improve the performance of microengines and the motion speeds to some extent, the preparation process is relatively complicated and the poor utilization of the expensive Pt material is also an obvious drawback. There exists a need for scalable synthetic methods to coat the surface of the microengines with precise control of the catalyst distribution. Most importantly, the size distribution of nanoparticle and efficient loading of the noble-metal catalyst should be of great importance to improve the performance of microengines.

We consider that a convenient method to commendably satisfy the requirements may be the combination of rolled-up nanotechnology and atomic layer deposition (ALD). ALD has emerged as an important technique of depositing thin films for a variety of applications [21].

* Correspondence: gshuang@fudan.edu.cn; yfm@fudan.edu.cn

²Department of Materials Science, Fudan University, Shanghai 200433, China
Full list of author information is available at the end of the article

Sequential self-limiting surface reaction steps enable excellent thickness control, conformal coating on highly complex nanostructures, and good uniformity over a large area [22]. The ALD of noble metals such as Pt has been shown to generate well-dispersed nanoparticles during the initial stages of growth [23–26]. This feature could be meaningful for catalytic engines since the nanoparticle array with large surface area and high surface-area-to-volume ratio can effectively improve the utilization efficiency of catalyst [27].

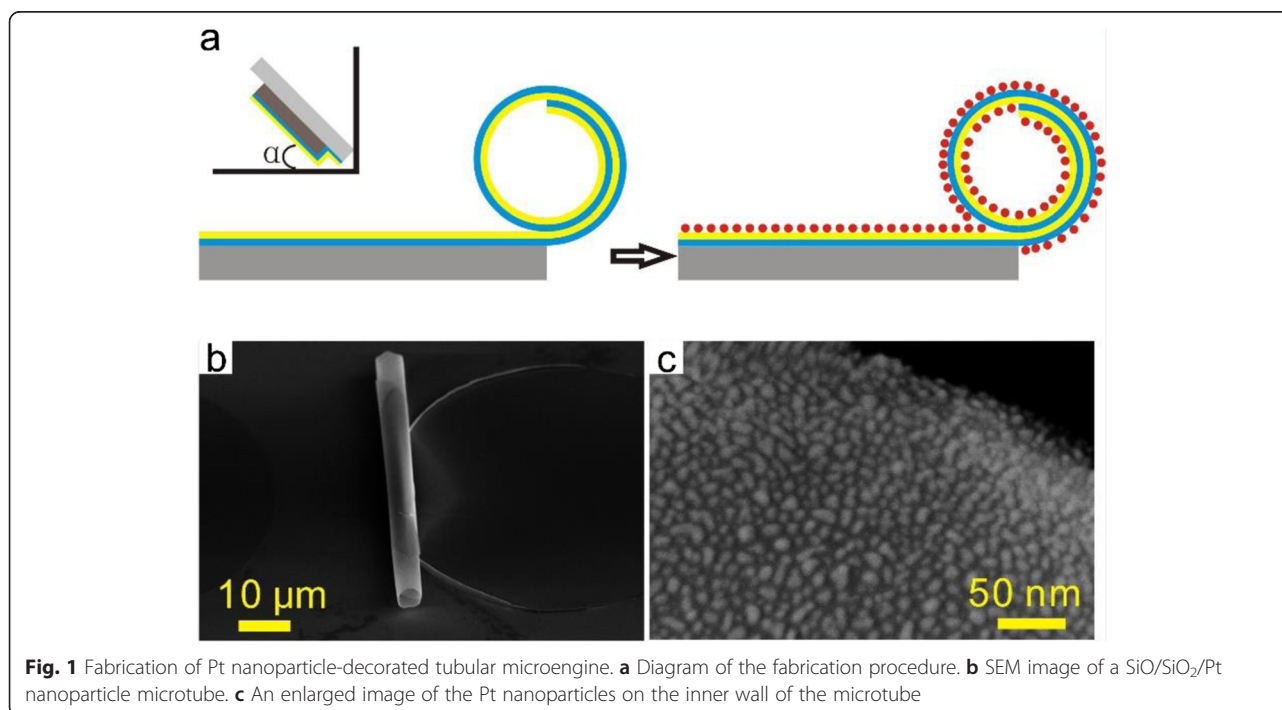
Here, we demonstrate a simplified approach using ALD of fabricating Pt nanoparticles for the mass production of highly efficient microtubular engines. The presence of Pt nanoparticles with different sizes and distributions on the walls of microengines results in promoted catalytic reaction efficiency. Correspondingly, the Pt nanoparticle-decorated microengines exhibit significant speed acceleration compare to the theoretical speed of smooth microengines with the same diameter and length. The high performance of current Pt nanoparticle-decorated microengines offers a great opportunity for designing and producing ultrapowerful micro-/nanomachines for practical applications like cargo and drug delivery.

Results and Discussion

Fabrication of Pt Nanoparticle-Decorated Tubular Microengine

Figure 1a illustrates the experimental procedure for the fabrication of Pt nanoparticle-decorated microengine. The fabrication strategy was based on rolled-up technology

using photoresist as a sacrificial layer (see the “Experimental Section” section for details) [12]. Briefly, bilayer nanomembranes with different thicknesses and thickness ratios (e.g., SiO/SiO₂ 5/20 nm, Ti/SiO₂ 20/10 nm, Ti/Co 10/10 nm, SiO₂/Ti 10/20 nm) were deposited on photoresist patterns via electron beam evaporation. After selective etching of the sacrificial layer, the bilayer was set free and the strain gradient causes rolling of the bilayer nanomembrane into microtube [12]. Geometrical parameters such as the length, diameter, and shape of the microtubes can be tuned on one hand by changing the dimensions of the photoresist patterns and on the other hand by controlling the angles, rates, and thicknesses during the depositions of the nanomembranes [28]. After formation of microtubes, Pt nanoparticles were coated on the tube wall by ALD, where two self-limiting and complementary reactions are used in an alternating sequence [29]. On the first cycle, the PtO_x was produced during piping in a pulse of O₂. Then, a pulse of methylcyclopentadienyl-(trimethyl) platinum(IV) ((MeCp)Pt(Me)₃) is forced into the generator’s chamber, which reacted with the PtO_x layer and O atoms are removed, leaving only Pt. On the next cycle, the unreacted precursor was removed and Pt surface was oxidized during the pulse of O₂, preparing it for the next cycle [30, 31]. Due to its high surface energy, Pt deposition on supports proceeds via an island growth mechanism (Volmer–Weber mechanism) during the initial stages of ALD processes [30, 31]. Ultimately, after a sufficient number of exposure cycles, the islands will merge to form a film. However, for applications in catalysis, it is typically



undesirable to obtain a continuous film: the island structure should be maintained because the islands/nanoparticles with a high surface-area-to-volume ratio should have better catalytic activity compared with flat layer [32, 33]. In current work, Pt nanoparticles were uniformly coated on the surface of the tube walls by precisely controlling the number of cycles adopted.

Figure 1b displays bird-view scanning electron microscopy (SEM) image of a typical 50- μm -long Pt nanoparticle-decorated SiO/SiO₂ microtube under low magnification. A close examination of such tubular structure (Fig. 1c) reveals that, unlike common rolled-up microtube with a Pt smooth surface [34], the current microtube is covered by nanoparticles with average diameters of ~ 10 nm. As will be illustrated below, such Pt nanostructure leads to a dramatically increased catalytic surface area [35] and corresponding improved propulsion efficiency [36].

We further investigated formation of Pt nanoparticles on different microtubular structures. Figure 2a–d shows that the microtubes of well-defined lengths and geometries by rolling different nanomembranes can be arranged into ordered arrays. Such arrays can be mass-produced by normal photolithography and this makes it easier to prepare a large number of microengines simultaneously [37]. As demonstrated in our previous work [12], the diameter can be tuned by changing the layer thicknesses, the thickness ratios, and the built-in strain in the nanomembrane. In present case, the SiO/SiO₂ microtubes have diameter of 5 μm and Ti/SiO₂ microtubes have larger diameter of 12 μm due to different nanomembrane thicknesses and stress gradient therein. In order to illustrate the Pt nanoparticles on the inner tube wall for details, Fig. 2e–h shows the corresponding SEM images. It is found that nanometer-scale islands nucleate on the wall of microtubes after ALD cycles. The energy dispersive X-ray spectra of the samples (not shown) clearly prove the presence of Pt on the tube walls. However, the nanoparticles on different top layer of nanomembranes (inner tube wall) show different sizes and morphologies after the same ALD process. The nanomembranes with oxide top layers (i.e., SiO/SiO₂ and Ti/SiO₂ bilayers) exhibit very flat and smooth surface and the Pt nanoparticles on them appear in the form of irregular shapes like ellipses and bars (Fig. 2e, f). On the other hand, the nanomembrane containing metallic layers (Ti/Co and SiO₂/Ti in present case) is relatively rough and uneven, and Pt nanoparticles in the form of small semi-spheres on the surface can be observed (Fig. 2g, h). We believe that the morphological difference in the bilayer nanomembranes is mainly due to different growth models and surface energies between oxide and metals during electron beam evaporation [38, 39]. In such incoherent growth condition, the growth of large particles/islands as a result of dissolution of small particles/islands can be explained by Ostwald ripening mechanism

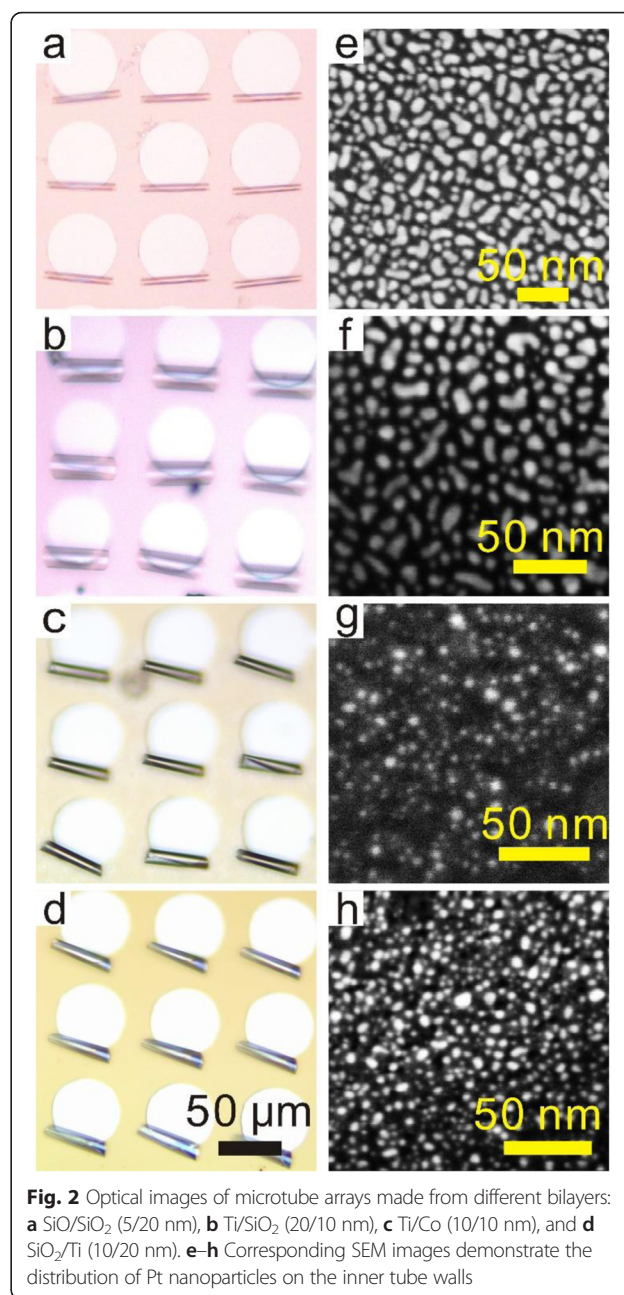


Fig. 2 Optical images of microtube arrays made from different bilayers: **a** SiO/SiO₂ (5/20 nm), **b** Ti/SiO₂ (20/10 nm), **c** Ti/Co (10/10 nm), and **d** SiO₂/Ti (10/20 nm). **e–h** Corresponding SEM images demonstrate the distribution of Pt nanoparticles on the inner tube walls

[38]. These factors also cause the change of the shapes of Pt nanoparticles when they are deposited on nanomembranes with oxide and metal top layer. However, it should be mentioned that, for the sake of simplicity, we suppose the nanoparticles are all in the shape of semi-spheres in the following model. This certainly introduces deviation in the model, but as we will discuss later, the experimental results can fit theoretical prediction well, suggesting that this simplicity is acceptable. Based on Fig. 2e–h, we have calculated the mean sizes of Pt nanoparticle on the inner wall (top layer). The results are 11, 10, 5, and 6 nm for nanoparticles on the surfaces of SiO/SiO₂, Ti/SiO₂, Ti/Co,

and SiO₂/Ti nanomembranes, respectively (Additional file 1: Figure S1). And the densities of nanoparticles are as high as 3.07×10^{15} , 4.62×10^{15} , and 1.85×10^{16} , and $3.18 \times 10^{16} \text{ m}^{-2}$, respectively. It is clear that the Pt nanoparticles on the inner tube wall of SiO/SiO₂ and Ti/SiO₂ microtubes are larger than those on the inner tube wall of Ti/Co and SiO₂/Ti microtubes, but the densities show the opposite result.

The Motion of Pt Nanoparticle-Decorated Tubular Microengine

Figure 3a–d shows time-lapse images of the movement of Pt nanoparticle-decorated SiO/SiO₂ microengines in

10 % H₂O₂ (see also Additional file 2: Video 1). Oxygen bubbles ejected from one large end of microengine through the decomposition of H₂O₂ and propelled the microengine in opposite direction [40]. It is worth noting that both inner and outer surfaces are covered with Pt nanoparticles after Pt coating by ALD, but we observed no O₂ bubbles generating on the outer surfaces of microengines. This indicates that O₂ molecules have different nucleation behaviors on the inner and outer surfaces. The similar phenomenon had also been found in single-component metal oxide tubular microengines controlled by UV light [41]. It is considered that the geometries of the microengines have significant

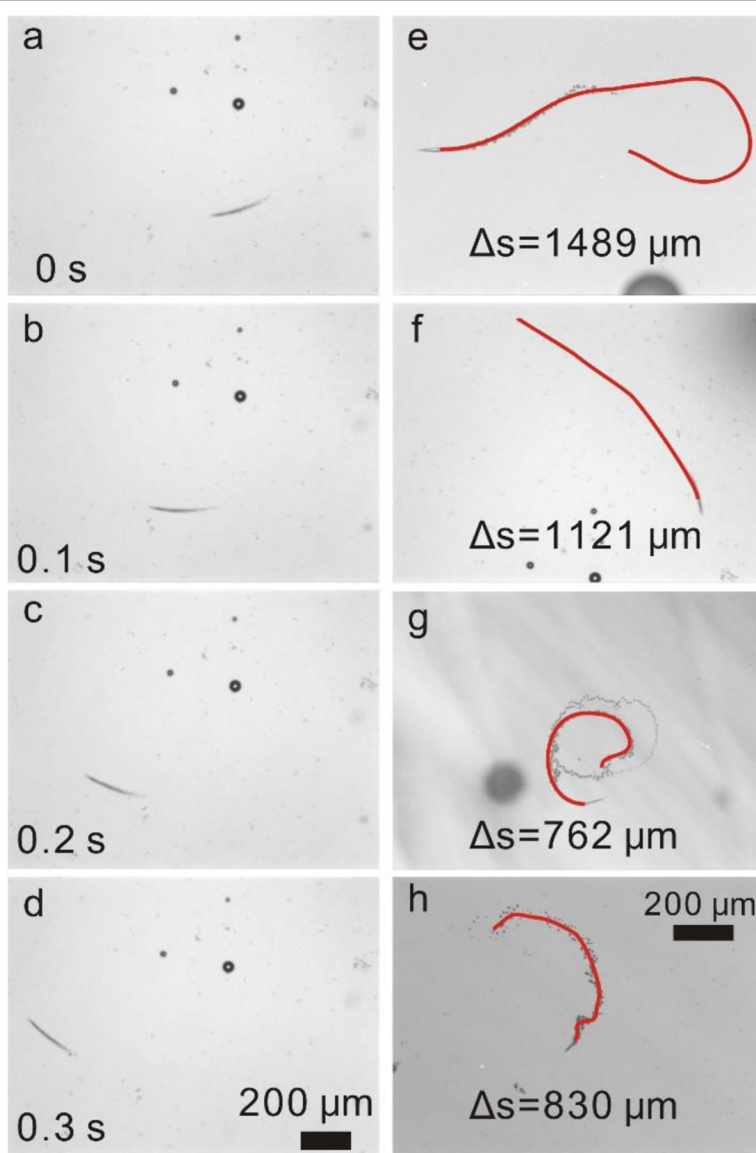


Fig. 3 a–d Selected motion images of SiO/SiO₂/Pt microengines at a 0, b 0.1, c 0.2, and d 0.3 s in 10 % H₂O₂ solution. e–h Trajectories of the four microengines decorated with Pt nanoparticles: e SiO/SiO₂, f Ti/SiO₂, g Ti/Co, and h SiO₂/Ti. The red trajectories were recorded over a time period of 0.5 s in 10 % H₂O₂

influence on bubble nucleation and generation. Generally, the bubbles can be formed on solid surfaces, if the gases reach heterogeneous nucleation energy [42]. Previous literature demonstrated that there are two factors determine the heterogeneous nucleation energy: the gas saturation concentration and the curvature of the surface [43]. The energy required for bubble formation on a flat surface is less than on a convex surface, and even less energy is required on a concave surface. It indicated that the gas produced on the concave surface of inner tube wall is much easier to nucleate compared than that on the convex surface of outer tube wall. In addition, different from other microengines such as Janus–motor [44] and Au-Pt nanorod [45], our microtubes can be used as a gas collecting chamber and O₂ molecules produced inside the microtube will easily reach the supersaturation concentration for the bubble nucleation due to the accumulative effect of the inner confined space [46]. The accumulated O₂ gas in the microtube can further facilitate the bubble nucleation. We noticed that the existence of Pt nanoparticles on the surface of the tube wall makes the catalytic decomposing reaction much more intense compared with smooth Pt layer, and high frequency bubble generation forms a long tail at the tube end. In our previous work [47], for a microtubular engine, we used the following Eq. (1) to calculate the oxygen productivity dV_{O_2}/dt :

$$dV_{O_2}/dt = nC_{H_2O_2}\pi RL \quad (1)$$

where n is O₂ production rate constant which was experimentally estimated to be $\approx 9.8 \times 10^{-4} \text{ ms}^{-1}$ in our previous work [46] and $C_{H_2O_2}$ is the concentration of H₂O₂. This equation is considered to be valid for the microengines with a smooth inner surface. However, for the current microengines decorated with Pt nanoparticles, the inner surface area is much bigger than $2\pi RL$. Apparently, the oxygen production is much higher than the microengines with smooth Pt layer, suggesting that Pt nanoparticle-decorated microengines can produce more oxygen. The corresponding bubble generation frequency makes the decorated microengines move in higher speed as we will explain in detail later. Detailed analysis of the video and time-lapse images demonstrates that the microengine was propelled at an ultrafast speed of around $3200 \mu\text{m s}^{-1}$ (Additional file 2: Video 1). According to the literature, for swimmer at low Reynolds number, the drag force (F) acted on the microengine is proportional to the motion speed (v) [47],

$$F = -\frac{2\pi\mu Lv}{\ln(X)-0.72} \quad (2)$$

where $X = 2L/R$ is a geometrical parameter (L and R are the length and radius of the microengine, respectively)

and μ is the fluid viscosity. The motion with faster speed means that the Pt-coated microengines need to overcome higher resistance. Moreover, the output power is proportional to the square of the motion speed since the output power is the product of the driving force and speed. In present case, one can deduce that the output power of Pt nanoparticle-decorated Ti/SiO₂ microengines is also remarkably increased due to its ultrafast speed, and quantitative analyses of the speed promotion will be given below. We believe that the higher output power could enable this kind of microengines to accomplish more complex tasks in the future. For instance, we observed a powerful microengine spewing tiny bubbles off their back and push along a big bubble in the front (see the Additional file 3: Video 2), suggesting potential applications of powerful microengines in the field of microdelivery [48] or smart drug delivery [49]. It is worth noting that the performance enhancement is not limited to SiO/SiO₂ microengine after decoration with Pt nanoparticles. Our results indicate that Pt nanoparticle decoration also leads to acceleration of other kinds of microtubular engines. In order to elucidate this phenomenon clearly, in Fig. 3e–f, we show the trajectories of four microengines moving in 10 % H₂O₂, extracting from the corresponding Additional files 4, 5, 6, and 7: Videos 3–6. One may note that the trajectories and the microbubble tails show unique geometries like linear, circular, and helical curves (Additional file 1: Figure S2). It is considered to be due to the imperfection in the microtubular structures, which generates a torque which is not parallel to the axis of microtubes resulting in different movement behaviors [40]. Quantitatively, the moving distances over a period of 0.5 s are 1489, 1121, 762, and 830 μm for Pt nanoparticle-decorated SiO/SiO₂, Ti/SiO₂, Ti/Co, and SiO₂/Ti microtubes, respectively (Fig. 3). We found that particle distribution and size have a great influence on the surface area and therefore the performance of microengines. The surface area of SiO/SiO₂/Pt, Ti/SiO₂/Pt, Ti/Co/Pt, and SiO₂/Ti/Pt microengines is 1.48, 1.80, 1.42, and 1.20 times larger, respectively, compared with smooth microtubular structure (Additional file 1: Figure S3), and thus, they demonstrated efficient catalytic effect, powerful propulsion thrust, and distinct moving trajectories, as shown in the Additional files 8, 9, 10 and 11: Videos 7–10. In addition, the enhanced surface area due to the existence of Pt nanoparticles also makes the microengines available to work in solution with low H₂O₂ concentration, and the motion of Pt nanoparticle-decorated microengines in 5 mL 10 % H₂O₂ after 24 h was shown in Additional file 12: Video 11. We experimentally found that the threshold H₂O₂ concentration for current Pt nanoparticle-decorated microengine can be as low as

~0.5 %. The time-lapse images in Additional file 1: Figure S4 display a Pt nanoparticle-decorated SiO/SiO₂ microengine moving in a 0.5 % H₂O₂ solution. Although the oxygen bubble generation frequency is low, the microengine is nonetheless self-propelled at a speed of ~100 μm/s.

The Experimental Results and Theoretical Model

To investigate the motion of decorated microengines in more details, we have calculated average speed of the four types of microengines based on statistics of 10 microengines in each case. Figure 4a shows the average speeds of the four types of Pt nanoparticle-decorated microengines moving in 5 and 10 % H₂O₂ solution. It is obvious that the average speeds of all four types increase with the concentration of H₂O₂ due to higher O₂ productivity (see below).

According to body deformation model [45], the bubbles propel the microengine in a stepwise manner and the

average speed of the smooth tubular microengines (v) can be theoretically predicted from Eq. (3)

$$v = \frac{9nC_{H_2O_2}X}{6 + X/(1nX - 0.72)}, \quad (3)$$

The above equation suggests that the average speed of a microengine is mainly determined by the geometrical parameter X under the certain H₂O₂ concentration, as plotted by the red dashed curve in Fig. 4b. One can see that the Pt nanoparticle-decorated SiO/SiO₂, Ti/SiO₂, and SiO₂/Ti microengines exhibit higher speeds compared with the theoretical prediction (1.38, 2, and 1.18 times, respectively), mainly due to the increase in the surface areas. If the surface areas are normalized (red, blue, and black squares in Fig. 4b), the experimental results can fit theoretical prediction very well if one notices that the surface areas were calculated by a simple approach (Additional file 1: Figure S3). This further proves that the larger surface area of the Pt nanoparticles (as calculated before) is mainly responsible for the highly efficient propulsion behavior of microengines, although the nanoparticle geometry may also affect the catalytic activity [32, 33]. Whereas in the case of Pt nanoparticle-decorated Ti/Co microengine (green square in Fig. 4b), the motion speed is slower than the theoretical prediction if the surface area is normalized. The surface area increased 1.42 times, but the speed increased only 1.26 times compared to the theoretical calculation. We assign this deviation to different surface morphology: the surface of the Ti/Co is unflat compared to other three samples, especially those with pure oxide bilayer nanomembrane, as we have mentioned above (see Fig. 2g). This may significantly influence the nucleation of gaseous microbubbles in the tubular chamber during catalytic motion and may also influence the dynamics of the microengine when it moves with high speed at low Reynolds number. In addition, we cannot rule out the possibility of the existence of electrochemical process in the O₂ production. The Ti/Co microengine is the only one in the current four samples with conductive tube wall. Although this needs further investigation, we consider that the electrochemical process therein may be one of the possible reasons leading to smaller O₂ productivity and corresponding slow motion speed.

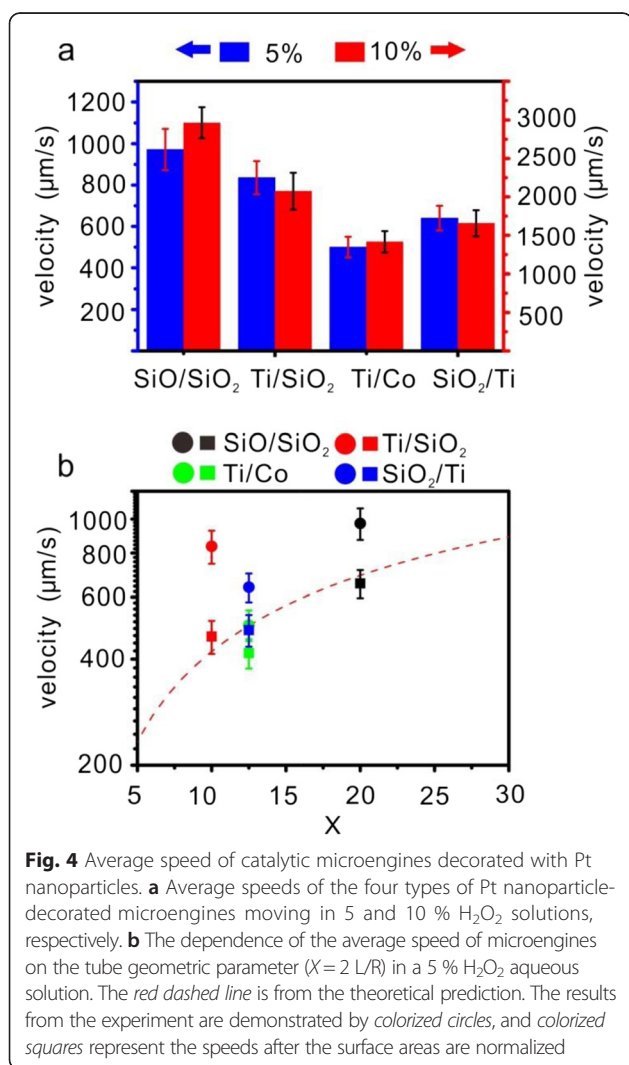


Fig. 4 Average speed of catalytic microengines decorated with Pt nanoparticles. **a** Average speeds of the four types of Pt nanoparticle-decorated microengines moving in 5 and 10 % H₂O₂ solutions, respectively. **b** The dependence of the average speed of microengines on the tube geometric parameter ($X = 2L/R$) in a 5 % H₂O₂ aqueous solution. The red dashed line is from the theoretical prediction. The results from the experiment are demonstrated by colored circles, and colored squares represent the speeds after the surface areas are normalized

Conclusions

We have demonstrated a convenient method to produce modified microtubular structures for high-speed microengines by employing ALD of Pt nanoparticles. Experimental results demonstrated that Pt nanoparticles coated on the walls of microtubes enabled a dramatic enhancement of the catalytic reaction and

correspondingly acceleration of motion speed due to increased surface area. The efficient propulsion performance of microengines holds considerable promise for catalysis support, drug/gene delivery, and medical imaging/diagnostics.

Methods

Fabrication of Microtubular Structures

Rolled-up microtubes consisting of different bilayer nanomembranes were prepared on polymer sacrificial layers. The 3510 T photoresist was spun coated on silicon substrate for 9 s at 600 rpm and 30 s at 3000 rpm then baked at 100 °C for 1 min, plus 10 min cooling down in the air. The resist got exposed in the mask-aligner for 10 s after the photo-mask has been aligned, and then resist was developed for 30~60 s. Ti/Co, SiO/SiO₂, SiO₂/Ti, and Ti/SiO₂ bilayers of 10/10, 5/20, 10/20, and 20/10 nm, respectively, were then deposited on photolithographically patterned circles and squares via e-beam evaporation. The samples were deposited with different rates (i.e., 1/1, 5/0.5, 1/2, and 2/1 Å s⁻¹, respectively) to build a strain gradient in nanomembrane under a high vacuum of 3.0 × 10⁻⁴ Pa. The samples were put in different angles inclined relatively to the horizontal to open an etching window at the far end of patterns. The intrinsic strain gradients in the bilayers after removing sacrificial photoresist layer by acetone made the bilayers roll into microtubular structures. To avoid collapse caused by the surface tension of the etchants, the samples were then dried in a critical point dryer (Leica CPD 030) using liquid CO₂ as the intermedium.

Pt Nanoparticle Deposition

Seventy cycles of Pt were deposited on the inner and outer surfaces of the prepared microtubes by ALD in a fluidized bed reactor. During the ALD process, (MeCp)Pt(Me)₃ and oxygen were used as precursors. Herein, the precursors (MeCp)Pt(Me)₃ and O₂ were pulsed into the reaction chamber by the carrier gas argon, and the temperature was kept at 70 °C. During the ALD process, the working pressure in the chamber was maintained at 5 mbar.

Motion Characterization

H₂O₂ solutions with different concentrations as fuel sources were added to activate the microengines at room temperature. An optical microscope (Olympus BX51) with an integrated camera was adopted to observe movement and locomotion of the microengines at a rate of 30 frame s⁻¹. With the assistance of Image J, a detailed investigation of trajectories and speed was carried out.

Additional files

Additional file 1: Figure S1. Pt nanoparticle size distribution on four different samples: **a** SiO/SiO₂ nanomembrane, **b** Ti/Co nanomembrane, **c** Ti/SiO₂ nanomembrane, and **d** SiO₂/Ti nanomembrane. **Figure S2.** Propulsion images showing the motion trajectories and corresponding tracking lines of Pt nanoparticle-decorated microengines. The right schematic diagrams sketch the corresponding force analysis of microengines. Movements: **a** circular and self-rotation, **b** helical, **c** linear, and **d** snake-like motions. Scale bars 200 μm. **Figure S3.** The SEM image of Pt nanoparticles on SiO/SiO₂ nanomembrane after being processed with the software Image J. **Figure S4.** Time-lapse images of a moving Pt nanoparticle-decorated SiO/SiO₂ microengine in solution with low H₂O₂ concentration of 0.5 %. The interval of each image is 0.1 s. (DOCX 525 kb)

Additional file 2: Video 1. (AVI 1578 kb)

Additional file 3: Video 2. (AVI 5877 kb)

Additional file 4: Video 3. (AVI 1283 kb)

Additional file 5: Video 4. (AVI 1571 kb)

Additional file 6: Video 5. (AVI 1731 kb)

Additional file 7: Video 6. (AVI 13004 kb)

Additional file 8: Video 7. (AVI 5991 kb)

Additional file 9: Video 8. (AVI 1910 kb)

Additional file 10: Video 9. (AVI 2853 kb)

Additional file 11: Video 10. (AVI 1708 kb)

Additional file 12: Video 11. (AVI 2158 kb)

Abbreviations

ALD: atomic layer deposition; (MeCp)Pt(Me)₃: methylcyclopentadienyl-(trimethyl) platinum(IV); SEM: scanning electron microscopy.

Competing Interests

The authors declare that they have no competing interests.

Authors' Contributions

YM conceived the idea of the experiments. CJ and HD performed the experimental work. CJ and GH explained the obtained results and wrote the paper. GH and CM gave the advice along the work. SD carried out the preparation and characterization of the samples. All authors read and approved the final manuscript.

Acknowledgements

This work was supported by the Natural Science Foundation of China (Nos. 5132220 and 51475093), Specialized Research Fund for the Doctoral Program of Higher Education (No. 20120071110025), and Science and Technology Commission of Shanghai Municipality (No. 14JC1400200).

Author details

¹School of Energy and Power Engineering, University of Shanghai for Science and Technology, Shanghai 200093, China. ²Department of Materials Science, Fudan University, Shanghai 200433, China. ³School of Microelectronics, Fudan University, Shanghai 200433, China.

Received: 18 April 2016 Accepted: 1 June 2016

Published online: 13 June 2016

References

- Mirkovic T, Zacharia NS, Scholes GD, Ozin GA (2010) Nanolocomotion—catalytic nanomotors and nanorotors. *Small* 6:159
- Gibbs JG, Zhao YP (2009) Autonomously motile catalytic nanomotors by bubble propulsion. *Appl Phys Lett* 94:163104
- Li J, Sattayasamitsathit S, Dong R, Gao W, Tam R, Feng X, Wang J (2014) Template electrosynthesis of tailored-made helical nanoswimmers. *Nanoscale* 6:9415
- Mei Y, Solovev AA, Sanchez S, Schmidt OG (2011) Rolled-up nanotech on polymers: from basic perception to self-propelled catalytic microengines. *Chem Soc Rev* 40:2109

5. Huang G, Wang J, Mei Y (2012) Material considerations and locomotive capability in catalytic tubular microengines. *J Mater Chem* 22:6519
6. Ibele M, Mallouk TE, Sen A (2009) Schooling behavior of light-powered autonomous micromotors in water. *Angew Chem Int Ed* 48:3308
7. Tottori S, Zhang L, Qiu F, Krawczyk KK, Franco-Obregón A, Nelson BJ (2012) Magnetic helical micromachines: fabrication, controlled swimming, and cargo transport. *Adv Mater* 24:811
8. Kagan D, Benchimol MJ, Claussen JC, Chuluun-Erdene E, Esener S, Wang J (2012) Acoustic droplet vaporization and propulsion of perfluorocarbon-loaded microbullets for targeted tissue penetration and deformation. *Angew Chem Int Ed* 124:7637
9. Wang H, Zhao G, Pumera M (2014) Beyond platinum: bubble-propelled micromotors based on Ag and MnO₂ catalysts. *J Am Chem Soc* 136:2719
10. Wang J (2013). *Nanomachines: fundamentals and applications*. John Wiley & Sons, Weinheim
11. Gao W, Sattayasamitsathit S, Orozco J, Wang J (2011) Highly efficient catalytic microengines: template electrosynthesis of polyaniline/platinum microtubes. *J Am Chem Soc* 133:11862
12. Mei Y, Huang G, Solovev AA, Ureña EB, Mönch I, Ding F, Schmidt OG (2008) Versatile approach for integrative and functionalized tubes by strain engineering of nanomembranes on polymers. *Adv Mater* 20:4085
13. Solovev AA, Mei Y, Bermúdez Ureña E, Huang G, Schmidt OG (2009) Catalytic microtubular jet engines self-propelled by accumulated gas bubbles. *Small* 5:1688
14. Sanchez S, Solovev AA, Schulze S, Schmidt OG (2011) Controlled manipulation of multiple cells using catalytic microrobots. *Chem Commun* 47:698
15. Solovev AA, Xi W, Gracias DH, Harazim SM, Deneke C, Sanchez S, Schmidt OG (2012) Self-propelled nanotools. *ACS Nano* 6:1751
16. Solovev AA, Sanchez S, Pumera M, Mei YF, Schmidt OG (2010) Magnetic Control of Tubular Catalytic Microrobots for the Transport, Assembly, and Delivery of Micro-objects. *Adv Funct Mater* 20:2430
17. Martín A, Jurado-Sánchez B, Escarpa A, Wang J (2015) Template electrosynthesis of high-performance graphene microengines. *Small* 11:3568
18. Laocharoensuk R, Burdick J, Wang J (2008) CNT-induced acceleration of catalytic nanomotors. *ACS Nano* 2:1069
19. Li J, Zhang J, Gao W, Huang G, Di Z, Liu R, Mei Y (2013) Dry-released nanotubes and nanoengines by particle-assisted rolling. *Adv Mater* 25:3715
20. Li J, Liu Z, Huang G, An Z, Chen G, Zhang J, Mei Y (2014) Hierarchical nanoporous microtubes for high-speed catalytic microengines. *NPG Asia Materials* 6:e94
21. Zaera F (2013) Nanostructured materials for applications in heterogeneous catalysis. *Chem Soc Rev* 42:2746
22. Li J, Liang X, King D M, Jiang YB, Weimer AW (2010) Highly dispersed Pt nanoparticle catalyst prepared by atomic layer deposition. *Appl Catal B-Environm* 97:220
23. Cheng N, Banis MN, Liu J, Riese A, Li X, Li R, Sun X (2015) Extremely stable platinum nanoparticles encapsulated in a zirconia nanocage by area-selective atomic layer deposition for the oxygen reduction reaction. *Adv Mater* 27:277
24. Elam JW, Zinovev A, Han CY, Wang HH, Welp U, Hryn JN, Pellin MJ (2006) Atomic layer deposition of palladium films on Al₂O₃ surfaces. *Thin Solid Films* 515:1664
25. Johansson A, Lu J, Carlsson JO, Boman M (2004) Deposition of palladium nanoparticles on the pore walls of anodic alumina using sequential electroless deposition. *J Appl Phys* 96:5189
26. King JS, Wittstock A, Biener J, Kucheyev SO, Wang YM, Baumann TF, Bent SF (2008) Ultralow loading Pt nanocatalysts prepared by atomic layer deposition on carbon aerogels. *Nano Lett* 8:2405
27. Zhou Y, Muhich CL, Neltner BT, Weimer AW, Musgrave CB (2012) Growth of Pt particles on the anatase TiO₂ (101) surface. *J Phys Chem C* 116:12114
28. Liu Z, Li J, Wang J, Huang G, Liu R, Mei Y (2013) Small-scale heat detection using catalytic microengines irradiated by laser. *Nanoscale* 5:1345
29. Christensen ST, Elam JW, Rabuffetti FA, Ma Q, Weigand SJ, Lee B, Bedzyk MJ (2009) Controlled growth of platinum nanoparticles on strontium titanate nanocubes by atomic layer deposition. *Small* 5:750
30. Ding SJ, Chen HB, Cui XM, Chen S, Sun QQ, Zhou P, Shen C (2013) Atomic layer deposition of high-density Pt nanodots on Al₂O₃ film using (MeCp)Pt(Me)₂ and O₂ precursors for nonvolatile memory applications. *Nanoscale Res Lett* 8:1
31. Rykaczewski K, Henry MR, Kim SK, Fedorov AG, Kulkarni D, Singamaneni S, Tsukruk W (2009) The effect of the geometry and material properties of a carbon joint produced by electron beam induced deposition on the electrical resistance of a multiwalled carbon nanotube-to-metal contact interface. *Nanotechnology* 21:035202
32. Levenspiel O (1999) Chemical reaction engineering. *Ind Eng Chem Res* 38:4140
33. Boudart M, Djéga-Mariadassou G (1984). Kinetics of heterogeneous catalytic reactions. Princeton University Press, Princeton
34. Sanchez S, Solovev AA, Mei Y, Schmidt OG (2010) Dynamics of biocatalytic microengines mediated by variable friction control. *J Am Chem Soc* 132:13144
35. Peng Q, Sun XY, Spagnola JC, Hyde GK, Spontak RJ, Parsons GN (2007) Atomic layer deposition on electrospun polymer fibers as a direct route to Al₂O₃ microtubes with precise wall thickness control. *Nano Lett* 7:719
36. Dasgupta NP, Liu C, Andrews S, Prinz FB, Yang P (2013) Atomic layer deposition of platinum catalysts on nanowire surfaces for photoelectrochemical water reduction. *J Am Chem Soc* 135:12932
37. Sanchez S, Solovev AA, Harazim SM, Schmidt OG (2010) Microrobots swimming in the flowing streams of microfluidic channels. *J Am Chem Soc* 133:701
38. Zinke-Allmang M, Feldman LC, Nakahara S (1987) Role of Ostwald ripening in islanding processes. *Appl Phys Lett* 51:975
39. Madras G, McCoy BJ (2003) Ostwald ripening in two dimensions: time dependence of size distributions for thin-film islands. *Phys Chem Chem Phys* 5:5459
40. Wang J, Gao W (2012) Nano/microscale motors: biomedical opportunities and challenges. *ACS Nano* 6:5745
41. Mou F, Li Y, Chen C, Li W, Yin Y, Ma H, Guan J (2015) Single-component TiO₂ tubular microengines with motion controlled by light-induced bubbles. *Small* 11:2564
42. Jones SF, Evans GM, Galvin KP (1999) Bubble nucleation from gas cavities—a review. *Adv Colloid Interface* 80:27
43. Huang W, Manjare M, Zhao Y (2013) Catalytic nanoshell micromotors. *J Phys Chem C* 117:21590
44. Gao W, Pei A, Feng X, Hennessy C, Wang J (2013) Organized self-assembly of Janus micromotors with hydrophobic hemispheres. *J Am Chem Soc* 135:998
45. Sundararajan S, Lammert PE, Zudans AW, Crespi VH, Sen A (2008) Catalytic motors for transport of colloidal cargo. *Nano Lett* 8:1271
46. Fletcher N (1958) Size effect in heterogeneous nucleation. *J Chem Phys* 29:572
47. Li J, Huang G, Ye M, Li M, Liu R, Mei Y (2011) Dynamics of catalytic tubular microjet engines: dependence on geometry and chemical environment. *Nanoscale* 3:5083
48. Kagan D, Laocharoensuk R, Zimmerman M, Clawson C, Balasubramanian S, Kang D, Wang J (2010) Rapid delivery of drug carriers propelled and navigated by catalytic nanoshuttles. *Small* 6:2741
49. Gao W, Kagan D, Pak OS, Clawson C, Campuzano S, Chuluun-Erdene E, Wang J (2012) Cargo-towing fuel-free magnetic nanoswimmers for targeted drug delivery. *Small* 8:460

Submit your manuscript to a SpringerOpen[®] journal and benefit from:

- Convenient online submission
- Rigorous peer review
- Immediate publication on acceptance
- Open access: articles freely available online
- High visibility within the field
- Retaining the copyright to your article

Submit your next manuscript at ► springeropen.com